Dossier

This paper is a part of the hereunder thematic dossier published in OGST Journal, Vol. 70, No. 6, pp. 909-1132 and available online here

Cet article fait partie du dossier thématique ci-dessous publié dans la revue OGST, Vol. 70, n°6, pp. 909-1132 et téléchargeable ici

Oil & Gas Science and Technology – Rev. IFP Energies nouvelles, Vol. 70 (2015), No. 6, pp. 909-1132

909 > *Editorial - Enhanced Oil Recovery (EOR), Asphaltenes and Hydrates*
Éditorial - EOR «récupération assistée du pétrole», Asphaltènes et Hydrates
D. Langevin and F. Baudin

ENHANCED OIL RECOVERY (EOR)

917 > *HP-HT Drilling Mud Based on Environmently-Friendly Fluorinated Chemicals*
Boues de forage HP/HT à base de composés fluorés respectueux de l'environnement
I. Henaut, D. Pasquier, S. Rovinetti and B. Espagne

931 > *Effective Viscosity in Porous Media and Applicable Limitations for Polymer Flooding of an Associative Polymer*
Viscosité effective dans des médias poreux et limites d'application de l'injection de polymères associatifs
P. Zhang, Y. Wang, Y. Yang, W. Chen and S. Bai

941 > *Dynamic Gelation of HPAM/Cr(III) under Shear in an Agitator and Porous Media*
Gélification dynamique de HPAM/Cr(III) sous cisaillement dans un agitateur et en milieu poreux
Y. Haiyang, W. Yefei, Z. Jian, L. Peng and S. Shenglong

951 > *Computer Modeling of the Displacement Behavior of Carbon Dioxide in Undersaturated Oil Reservoirs*
Modélisation par ordinateur du comportement de déplacement du dioxyde de carbone dans des réservoirs d'huile non saturés
B. Ju, Y.-S. Wu and J. Qin

967 > *Predicting CO_2 Minimum Miscibility Pressure (MMP) Using Alternating Conditional Expectation (ACE) Algorithm*
Prédiction de la pression miscibilité minimum (MMP) du CO_2 en utilisant un algorithme basé sur l'ACE *(Alternating Conditional Expectation)*
O. Alomair, A. Malallah, A. Elsharkawy and M. Iqbal

983 > *Towards the Development of Bitumen Carbonates: An Integrated Analysis of Grosmont Steam Pilots*
Vers le développement des carbonates bitumineux : une analyse intégrée des pilotes vapeur de Grosmont
C.C. Ezeuko, J. Wang, M.S. Kallos and I.D. Gates

1007> *A Novel Model of Foam Flooding Considering Multi-Factors for Enhancing Oil Recovery*
Un nouveau modèle d'injection de mousse considérant de multiples facteurs afin d'améliorer la récupération de pétrole
J. Wang, H. Liu, H. Zhang, G. Zhang, P. Liu and K. Sepehrnoori

1025> *Testing of Snorre Field Foam Assisted Water Alternating Gas (FAWAG) Performance in New Foam Screening Model*
Vérification des performances de la méthode FAWAG (*Foam Assisted Water Alternating Gas)* sur le champ de Snorre, en Norvège, avec un nouveau modèle de sélection des mousses
P. Spirov and S. Rudyk

ASPHALTENES

1035> *Structural Study of Asphaltenes from Iranian Heavy Crude Oil*
Étude structurale d'asphaltènes de pétrole brut lourd iranien
L. Davarpanah, F. Vahabzadeh and A. Dermanaki

1051> *Experimental Study and Mathematical Modeling of Asphaltene Deposition Mechanism in Core Samples*
Étude expérimentale et modélisation mathématique du mécanisme de déposition d'asphaltène dans des carottes de forage
T. Jafari Behbahani, C. Ghotbi, V. Taghikhani and A. Shahrabadi

1075> *Prediction of the Gas Injection Effect on the Asphaltene Phase Envelope Prévision*
Prévision de l'effet d'injection de gaz sur l'enveloppe de phase des asphaltènes
P. Bahrami, R. Kharrat, S. Mahdavi and H. Firoozinia

HYDRATES

1087> *Methane Hydrate Formation and Dissociation in the Presence of Silica Sand and Bentonite Clay*
Formation et dissociation d'hydrates de méthane en présence de sable de silice et d'argile de bentonite
V. Kumar Saw, G. Udayabhanu, A. Mandal and S. Laik

1101> *Prediction of Mass Flow Rate in Supersonic Natural Gas Processing*
Prédiction du débit massique dans les applications de traitement supersonique du gaz naturel
C. Wen, X. Cao, Y. Yang and Y. Feng

1111> *Experimental Study on Hydrate Induction Time of Gas-Saturated Water-in-Oil Emulsion using a High-Pressure Flow Loop*
Étude expérimentale sur le temps d'induction d'hydrate d'une émulsion eau-en-huile saturée en gaz en utilisant une boucle à circulation sous haute pression
X.F. Lv, B.H. Shi, Y. Wang, Y.X. Tang, L.Y. Wang and J. Gong

1125> *Hollow Silica: A Novel Material for Methane Storage*
La silice creuse : un nouveau matériau pour le stockage de méthane
V.D. Chari, P.S.R. Prasad and S.R. Murthy

IFP Energies nouvelles

Oil & Gas Science and Technology – Rev. IFP Energies nouvelles, Vol. 70 (2015), No. 6, pp. 1051-1074

DOI: 10.2516/ogst/2013128

Experimental Study and Mathematical Modeling of Asphaltene Deposition Mechanism in Core Samples

T. Jafari Behbahani[1,2], C. Ghotbi[1]*, V. Taghikhani[1] and A. Shahrabadi[2]

[1] *Department of Chemical and Petroleum Engineering, Sharif University of Technology, Tehran - Iran*
[2] *Research Institute of Petroleum Industry (RIPI), Tehran - Iran*
e-mail: jafaribehbahani@che.sharif.ir - ghotbi@sharif.edu - taghikhani@sharif.edu - sharabadia@ripi.ir

* Corresponding author

Résumé — Étude expérimentale et modélisation mathématique du mécanisme de déposition d'asphaltène dans des carottes de forage — Les études expérimentales présentées dans ce document ont été effectuées afin de déterminer les effets de la déposition d'asphaltène sur la réduction de la perméabilité et de la porosité d'échantillons rocheux de carbonate, de grès et de dolomite en utilisant un échantillon de pétrole brut de fond de puits proche des conditions du réservoir, tandis que dans la majorité des travaux précédents un mélange d'huile recombinée (mélange de pétrole dégazé et des gaz associés) est injecté dans un échantillon de forage dans des conditions très éloignées de celles du réservoir. Les effets du taux d'injection de pétrole sur la déposition d'asphaltène et la réduction de la perméabilité ont été étudiés. Les résultats expérimentaux montrent qu'une augmentation du débit d'injection de pétrole peut causer une augmentation du dépôt d'asphaltène et une réduction de la perméabilité. Il est aussi observé que, pour des débits d'injection plus faibles, une diminution monotone de la perméabilité des échantillons rocheux peut être obtenue en augmentant le débit d'injection, alors que pour des débits d'injection plus élevés, après une diminution de la perméabilité de la roche, une tendance à l'augmentation est observée avant d'atteindre un état stationnaire. Les résultats expérimentaux montrent aussi que le type de roche peut affecter la quantité d'asphaltène déposée, et que la déposition d'asphaltène est liée à différents mécanismes dans les carottes de forage de grès et de carbonate. Il est mis en évidence que les mécanismes d'adsorption et de colmatage jouent un rôle plus important dans les carottes de carbonate que dans ceux de grès. Ces résultats indiquent que les volumes de pore du pétrole brut injecté sont plus élevés dans les échantillons de grès que dans ceux de carbonate. On peut ainsi en déduire que trois types de dépôts peuvent avoir lieu durant l'injection de pétrole brut : un dépôt continu pour les forages à faible perméabilité, un colmatage lent et progressif pour les forages à haute perméabilité et un dépôt progressif pour les forages à moyenne perméabilité. Les résultats expérimentaux indiquent ainsi qu'une augmentation de la pression de production provoque une augmentation des endommagements des carottes de forage. Ceux-ci montrent aussi que la quantité d'asphaltène restante dans les carottes de carbonate est plus élevée que celle restante dans les carottes de grès. De plus, des micrographies MEB (Microscopie Électronique à Balayage) des carottes de carbonate indiquent que la formation d'agglomérats d'asphaltène est plus importante dans ces échantillons que dans ceux en grès durant l'épuisement naturel. Il peut être conclu à partir des résultats de modélisation que les modèles proposés basés sur le mécanisme d'absorption à l'équilibre multicouches et quatre équations de bilan de matière sont plus précis

que ceux obtenus à partir du mécanisme d'absorption à l'équilibre monocouche et deux équations de bilan de matière : ces résultats sont en accord avec les données expérimentales d'épuisement naturel présentées dans cette étude et dans la littérature.

Abstract — Experimental Study and Mathematical Modeling of Asphaltene Deposition Mechanism in Core Samples *— In this work, experimental studies were conducted to determine the effect of asphaltene deposition on the permeability reduction and porosity reduction of carbonate, sandstone and dolomite rock samples using an Iranian bottom hole live oil sample which is close to reservoir conditions, whereas in the majority of previous work, a mixture of recombined oil (a mixture of dead oil and associated gas) was injected into a core sample which is far from reservoir conditions. The effect of the oil injection rate on asphaltene deposition and permeability reduction was studied. The experimental results showed that an increase in the oil injection flow rate can result in an increase in asphaltene deposition and permeability reduction. Also, it can be observed that at lower injection flow rates, a monotonic decrease in permeability of the rock samples can be attained upon increasing the injection flow rate, while at higher injection rates, after a decrease in rock permeability, an increasing trend is observed before a steady-state condition can be reached. The experimental results also showed that the rock type can affect the amount of asphaltene deposition, and the asphaltene deposition has different mechanisms in sandstone and carbonate core samples. It can be seen that the adsorption and plugging mechanisms have a more important role in asphaltene deposition in carbonate core samples than sandstone core samples. From the results, it can be observed that the pore volumes of the injected crude oil are higher for sandstone cores compared with the carbonate cores. Also, it can be inferred that three depositional types may take place during the crude oil injection, i.e., continuous deposition for low-permeability cores, slow, steady plugging for high-permeability cores and steady deposition for medium-permeability cores. It can be seen from the experimental results that damage to the core samples was found to increase when the production pressures were increased. The experimental results show that the amount of remaining asphaltene in carbonate core samples is higher than those in sandstone core samples. Also, SEM (Scanning Electron Microscopy) micrographs of carbonate core samples showed the formation of large clusters of asphaltene in comparison with sandstone core samples during natural depletion. It can be seen from the modeling results that the proposed model based on the multilayer adsorption equilibrium mechanism and four material balance equations is more accurate than those obtained from the monolayer adsorption equilibrium adsorption mechanism and two material balance equations, and is in agreement with the experimental data of natural depletion reported in this work and with those reported in the literature.*

NOMENCLATURE

C_{sf}	Mass of suspended asphaltenes per mass of the oil phase
C	Experimental concentration (in this case, in mol/L)
C_A	Volume fraction of the suspended asphaltene precipitates in the liquid phase
D_{pt}	Average pore throat diameter
D_{ptcr}	Critical pore throat diameter, assumed constant
E_A	Volume fraction of the deposited asphaltene in the bulk volume of the porous media
E_{ad}	Fractional pore volume of asphaltene adsorbed
f	Fugacity
K_a	Ratio of adsorption/desorption rate constants
K	Permeability
k_1	First adsorption step parameter (in our case, this step is taken to be adsorption of asphaltenes in solution to the surface of the rock)
k_2	Second adsorption step parameter (in our case, this step is taken to be the adsorption of asphaltenes in solution to those asphaltenes already adsorbed to the rock)
R	Gas constant
S_{oi}	Initial oil saturation
S_{wi}	Initial water saturation
n	Mean aggregation number of the adsorbed asphaltenes (in the modified model)
u	Internal energy
u_L	Flux of the liquid phase
v	Molar volume
v_L	Interstitial velocity of the liquid phase

v_c	Critical interstitial velocity of the liquid phase (cm/s)
w_{AL}	Dissolved asphaltene in the liquid phase
W_{asp}	Asphaltene content of the bottom hole live oil
w_G	Mass fraction of gas
w_{OL}	Mass fraction of the oil in the liquid phase
W_{sa}	Mass of adsorbed asphaltene per mass of rock
w_{SAL}	Mass fractions of the suspended asphaltene precipitates
$W_{sa,\ max}$	Maximum adsorbed mass fraction, mg/g
w_{WL}	Mass fraction of water in the liquid phase

Greek Symbols

Ø	Porosity
M	Viscosity
ρ	Density
Γ	Amount of adsorbed substance in mol/L
Γ_∞	Maximum possible adsorption for the whole isotherm
α	Surface deposition rate coefficient, sec^{-1}
β	Entrainment rate coefficient, cm^{-1}
γ	Plugging deposition rate coefficient, cm^{-1}
σ	Snowball-effect deposition constant
μ_p	Chemical potential
δ_p	Solubility parameter of a liquid
Φ_s	Volume fraction of solvent (liquid oil)

Subscripts

AAD	Average absolute deviation
cal	Calculated
exp	Exponential function
O	Oil phase
P_{res}	Reservoir pressure
Q	Flow rate
T_{res}	Reservoir temperature

INTRODUCTION

Asphaltenes and resins are the polar fractions of crude oil that can be separated by addition of low-molecular-weight *n*-alkanes. By definition, asphaltenes are the fraction of a crude oil that is soluble in toluene and insoluble in an *n*-alkane, typically pentane or heptane. These fractions are formed by molecules with a polyaromatic structure containing paraffinic and naphthenic chains, as well as oxygen, nitrogen and sulfur as functional groups or heteroatoms. On the other hand, asphaltenes are heavy hydrocarbon molecules that are in colloidal suspension in the oil, stabilized by resins adsorbed on their surface [1]. Asphaltenes can reduce the hydrocarbon effective mobility by plugging pore throats, thus reducing the rock permeability, altering the formation wettability from water-wet to oil-wet and increasing the reservoir fluid viscosity by forming a colloidal solution in the oil phase [2]. The processes of asphaltene precipitation and deposition in porous media have various effects on oil flow during primary oil production and enhanced oil recovery processes. The natural depletion of a reservoir may cause the precipitation and deposition of asphaltenes, decreasing the productivity of wells during primary oil recovery. The majority of existing work studies the asphaltene deposition during core flooding using the injection of recombined oil (a mixture of dead oil and associated gas) into the core and/or with static systems and in the absence of reservoir rocks [3-5]. Therefore, such results are not applicable to the dynamic conditions which are related to the complex interactions between the asphaltenes and the rock surface. Asphaltene precipitation and deposition are two different processes and are governed by different mechanisms. The asphaltene deposition is governed by four mechanisms; surface deposition, entrainment, plugging and adsorption (surface excess or Langmuir theory) [6-12]. When precipitation occurs, asphaltene particles are aggregated and a new solid phase is generated in the oil flow, whereas when deposition takes place on the rock, this can change the wettability of the reservoir formation and reduce oil production [13]. The asphaltene deposition phenomenon is described using several mathematical models that have been proposed for the prediction of porosity and permeability reduction of porous media [14-19]. These models are based on two different parallel pathways with small and large pore sizes [20]. Most models are capable of correlating the permeability reduction experimental data using adjustable parameters and include the flow continuity equation, a mass balance equation and a kinetic equation. Other models based on network modeling theory have also been developed to describe the deposition of asphaltene in reservoir rock [21, 22].

In short, due to the complexity of asphaltene deposition on the rock surface, very few experimental results currently exist on asphaltene deposition under dynamic conditions using live reservoir fluid in porous media. The majority of existing work addresses the deposition of asphaltenes using dead residual oil or recombined oil [6, 23-25], while it is well-known that the asphaltene in bottom hole live oil is different than that of recombined oil [26]. In this work, an Iranian bottom hole live oil sample was used under dynamic conditions in porous

TABLE 1
Studied live reservoir fluid compositions

Components	Dead residual oil (mol%)	Associated gas (mol%)	Live reservoir fluid (mol%)	Components	Dead residual oil (mol%)	Associated gas (mol%)	Live reservoir fluid (mol%)
H_2S	0	0	0	*n*_C_5	1.35	1.88	1.59
N_2	0	0.67	0.3	C_6	11.19	1.62	6.95
CO_2	0	4.12	1.83	C_7	6.87	0.63	4.1
C_1	0	51.19	22.7	C_8	6.84	0.15	3.88
C_2	0.51	17.94	8.24	C_9	4.47	0.01	2.49
C_3	1.17	12.38	6.14	C_{10}	7.24	0	4.03
*i*_C_4	0.52	2.02	1.19	C_{11}	5.13	0	2.85
*n*_C_4	1.94	5.7	3.61	C_{12}^+	51.64	0	28.74
*i*_C_5	1.14	1.68	1.38	Total	100	100	100

media for investigation of the effect of several parameters and different production conditions such as crude oil type, the flow rate of the oil, rock type and production pressure on asphaltene deposition. Also, the performance of the proposed model based on the multilayer adsorption equilibrium mechanism was studied in more detail and compared with the Wang and Civan [7] model based on the mechanical plugging mechanism and the asphaltene deposition model based on the monolayer adsorption equilibrium mechanism.

1 EXPERIMENTAL SECTION

1.1 Materials

In the majority of previous work, a mixture of recombined oil (a mixture of dead oil and associated gas) was injected into a core sample which is far from reservoir conditions. In this work, a bottom hole live oil sample from an Iranian reservoir in the Southeast region of Iran which is close to reservoir conditions was used. This reservoir has a serious asphaltene deposition problem during production conditions. The oil density and viscosity of the bottom hole live oil sample were measured to be 0.7674 g/cc and 4.35 cP at the reservoir pressure, respectively. The asphaltene content of the live reservoir fluid was measured to be wasp = 16.3 wt% using the SARA analyses. The compositional analysis result of this crude oil was obtained using the gas chromatography method and is given in Table 1.

A reservoir brine sample was collected from the same oilfield, cleaned, and analyzed. Its detailed physical and chemical properties are listed in Table 2.

TABLE 2
Physical and chemical properties of reservoir brine sample

Viscosity (CST at 40°C)	0.92
pH at 20°C	6.5
Oil (mg/L)	4
Chemical oxygen demand as O_2 (mg/L)	1 216
Biological oxygen demand as O_2 (mg/L)	530
Total suspended solids (mg/L)	352
Chloride (mg/L)	123 100
$CaCO_3$ (mg/L)	177
Sulfate (mg/L)	291
Total dissolved solids (mg/L)	202 050
Potassium (g/L)	1.1
Sodium (g/L)	60
Calcium (mg/L)	13 280
Magnesium (mg/L)	1 262
Iron (mg/L)	42
Strontium (g/L)	0.58
Lithium (mg/L)	13
Sulfide (mg/L)	7.2
Barium (mg/L)	1.2

TABLE 3
Characteristics of the various studied cores

Sample No.	Type of core	Length (cm)	Diameter (cm)	Porosity (%)	Permeability (mD)	Grain density (g/cm^3)	Weight (g)	PV
1	Carbonate	4.5	3.7	26	2.7	—	103.8	13.5
2	Dolomite	5.1	3.8	22.5	106.6	2.68	118.5	12.3
3	Sandstone	5.96	3.7	13.15	22.8	2.65	150.8	8.5

Various carbonate and sandstone cores with a cylindrical shape with lengths ranging from 4 to 6 cm and constant diameter equal to 4 cm were extracted at various depths of the Iranian wells, then characterized and tested in the EOR Research Center laboratory, Research Institute of Petroleum Industry (RIPI). All the cores investigated were cleaned prior to their use, by using various solvents (Soxhlet extraction with xylene, methanol and chloroform) according to the ASTM D2172 procedure. Their characteristics, including their porosities, permeabilities and pore volumes, were measured and are shown in Table 3.

1.2 Methods

1.2.1 Gas and Liquid Chromatography

When the live reservoir fluid sample was flashed in atmospheric conditions, vapor and liquid phases were analyzed by means of the High-Temperature Gas Chromatography (HTGC) technique. To analyze the lighter fraction up to C9 (including CO_2, H_2S and N_2) a high-temperature gas chromatograph (three packed columns and one capillary column) with thermal conductivity and flame ionization detectors was used, while the residual liquid was analyzed up to C12 with another high-temperature gas chromatograph (a capillary column) that included a flame ionization detector.

1.2.2 SARA Analyses of the Crude Oil

The constituents of crude oils are typically classified by solubility: Saturates, Aromatics, Resins and Asphaltenes (SARA) [27]. For SARA fraction analysis, the asphaltene fraction was extracted from crude oil by precipitation with *n*-heptane as described by the ASTM D3279-97 procedure. Subsequent elution with a series of increasingly polar solvents as the mobile phase yields saturates (eluted with a nonpolar solvent such as hexane), followed by the elution of aromatics with toluene, and the resins are separated with a more polar solvent.

TABLE 4
SARA test results of the studied reservoir fluid

Type of group	Live reservoir fluid	Residual oil
Saturate (wt%)	32.61	37.8
Aromatic (wt%)	43.48	46.2
Resin (wt%)	7.61	5.9
Asphaltene (wt%)	16.3	10.1

The SARA analysis results of live reservoir fluid are shown in Table 4.

1.2.3 Live Reservoir Fluid Viscosity

To determine the viscosity behavior of the reservoir fluid, at the studied temperature and different pressures, a constant force electromagnetic viscometer (maximum working pressure of 137.9 MPa, maximum temperature of 463.2 K) was used. The viscosity behavior of the live reservoir fluid is shown in Figure 1.

1.2.4 The PVT and Phase Behavior of the Live Reservoir Fluid

To determine the PVT and phase behavior of the live reservoir fluid, various experiments were conducted on the reservoir fluid, including constant mass expansion, differential vaporization and a separator test (DBR, VINCI PVT Cell). In these experiments, saturation pressure, relative volume, oil compressibility, the solution gas-oil ratio, the liberated gas-oil ratio, the oil formation volume factor and oil density were determined. In Tables 5 to 7, the PVT characteristics and phase behavior (constant mass expansion and differential vaporization results) of the studied live reservoir fluid are shown.

Also, the variation of relative volume, oil compressibility, the solution gas-oil ratio, the liberated gas-oil ratio, the oil formation volume factor and oil density with pressure are shown in Figures 2-4.

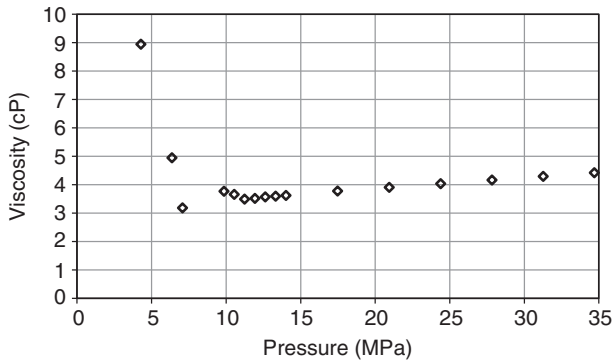

Figure 1

The viscosity behavior of the studied live reservoir fluid.

TABLE 5

PVT characteristics and phase behavior of the studied reservoir fluid

Reservoir pressure, P_{res} (MPa)	33
Reservoir temperature, T_{res} (°C)	96
Molar weight of the live reservoir fluid (g/mol)	182
Specific gravity of the live reservoir fluid	0.77
Molar weight of the heavy group (live reservoir fluid), C_{12}^{+} (g/mol)	491
Specific gravity of the heavy group (live reservoir fluid), C_{12}^{+}	0.99
Molar weight of the heavy group (dead residual oil), C_{12}^{+} (g/mol)	395

TABLE 6

Summary of constant mass expansion data for the studied live reservoir fluid

Saturation pressure	MPa	9.85
Solution GOR	SCF/STB	341.63
Density of total gas evolved	g/L	1.38
API gravity of residual oil	°API	20.29
Specific gravity of residual oil	60/60°F	0.93

TABLE 7

Summary of differential vaporization data for the studied live reservoir fluid

Solution GOR	SCF/STB	360.34
Density of total gas evolved	g/L	1.34
Oil density @ sat. pressure	g/cc	0.75
Oil density @ reservoir pressure	g/cc	0.77
Oil gravity of residual oil	°API	20.03
Specific gravity of residual oil	15/15°C	0.93
Oil viscosity @ sat. pressure	cP	3.50
Oil viscosity @ reservoir pressure	cP	4.36

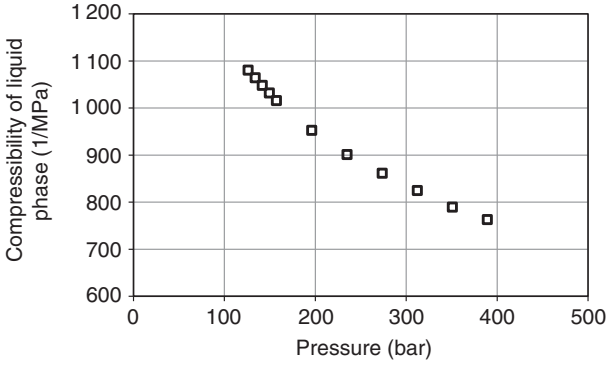

Figure 2

Variation of compressibility of liquid phase *versus* pressure for the studied live reservoir fluid.

1.3 Experimental Apparatus

Figure 5 shows the schematic of the experimental setup used in this work in order to determine the effect of asphaltene deposition on the properties of a reservoir rock.

This setup consists mainly of the following devices:

– an automatic displacement pump (*Vinci*, p = 70 MPa, accuracy = 0.000687 MPa) was used to displace the crude oil and reservoir brine through the composite reservoir core plugs inside a core holder (*Temco*);
– three high-pressure stainless steel cylinders (500-10-P-316-2, *DBR*, Canada) were used to store and deliver

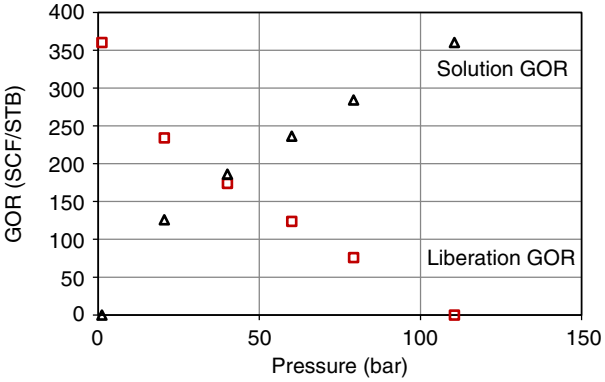

Figure 3

GOR results for the studied live reservoir fluid.

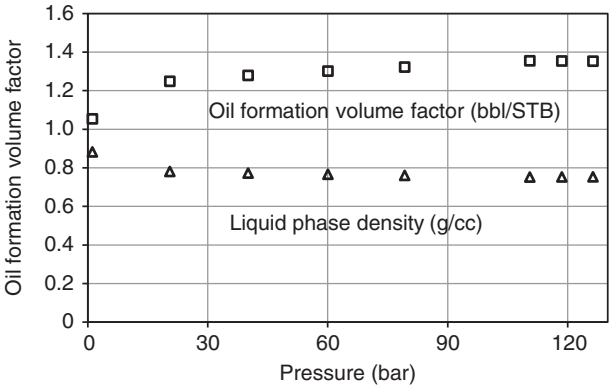

Figure 4

Differential liberation results *versus* pressure for the studied live reservoir fluid.

the live reservoir fluid, dead residual oil and reservoir brine, respectively (*DBR*, capacity of 500 mL);

– the core holder (*Temco*, p = 70 MPa, T = 150°C) holds a core through a sleeve. A constant overburden pressure was applied around this sleeve, which was always kept 5 MPa higher than the inlet pressure of the core holder. The inlet and outlet ports of the core holder were connected to the pressure transducer. The inlet ports of the core holder were also connected to the positive displacement pump. Two cylinders containing the live reservoir fluid sample allowed injection of samples inside the core holder. The positive displacement pump was operated at a constant rate or in pressure mode. The outlet port of the core holder was connected to the fractional collector through a back-pressure regulator for collection of produced fluids from the core.

The pressure drop during the core flood tests was measured with a digital pressure indicator. The core flooding system was thermoregulated by means of an air-bath oven. An important feature was the possibility of continuous measurement of the pressure drop along sections of the porous medium. The annular space between the sleeve and the body was filled with paraffin oil through which the confining pressure is applied on the external surface of the sleeve. The advantage of this setup is the uniform pressure in both axial and radial directions:

– a pressure transducer (*Jumo*, accuracy = 0.05);
– a back-pressure regulator (*Jeafer DBR*, p = 70 MPa, T = 250°C). The regulator was used to maintain the prespecified injection pressure inside the core holder during each flooding test;
– an overburden pump (*Enerpac*, p = 70 MPa);
– an air-bath oven (*Vinci*, T = 200°C);
– rigid valves;
– a data acquisition system (Logger screen 500 *Jumo*: pressure, temperature, volume).

1.4 Experimental Procedure

The reservoir core plugs were cleaned with toluene, methanol and chloroform in sequence to remove hydrocarbons, salts and clays, respectively. Then, the reservoir core plugs were dried and vacuumed at 0.7 bar for one hour, and the reservoir brine was imbibed to measure the pore volume of the reservoir core plugs. Afterward, the reservoir brine was injected at different rates (1-30 cc/h) to determine the water permeability of the core plugs. As listed in Table 3, the measured porosity was in the range of φ = 13.15-26% and the measured absolute permeability was in the range of k = 2.7-106.6 mD.

Then, reservoir brine was displaced by the live reservoir fluid until irreducible water saturation. After the core plugs were fully saturated with the crude oil, the live reservoir fluid was injected into the core plugs and several flooding tests were conducted. Then, the differential pressure (ΔP) between the inlet and outlet of the core holder was measured by a digital pressure indicator and was indicated by the data acquisition system at preset time intervals.

To study the effect of production pressure, the production pump was adjusted to 15 MPa and the injected pump to various pressures. The live reservoir fluid was injected into the core and attained stabilized conditions within a few minutes. Then, the procedure of gradual pressure reduction was followed throughout the experiment. The injection pressure used in this experiment was in the range of 50-41 MPa with temperature at 70°C using live reservoir fluid. There was no flow of

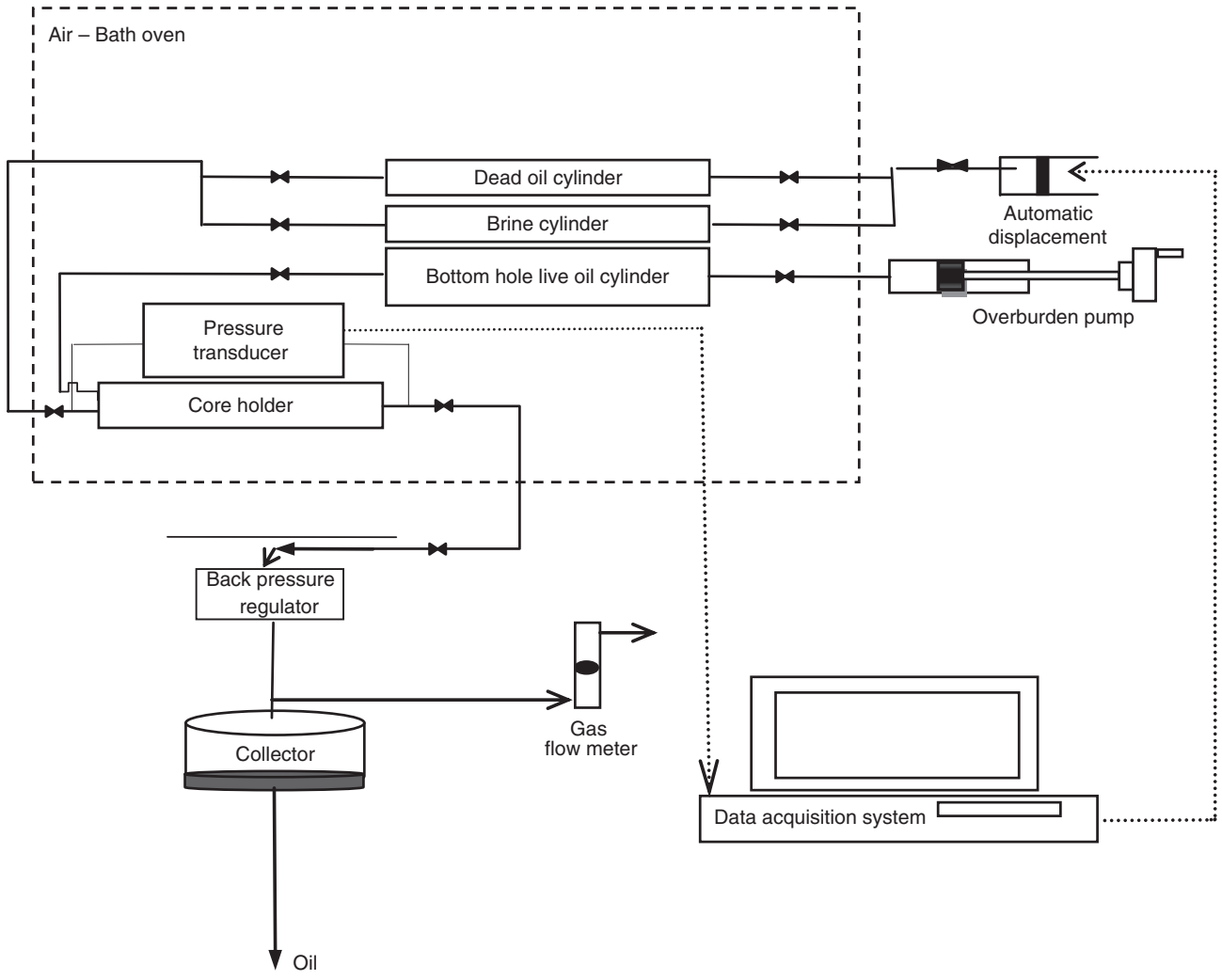

Figure 5

Schematic of core flooding apparatus.

crude oil at injection pressures lower than 41 MPa. In total, 13 sets of flooding tests were performed. Table 8 shows the experimental conditions.

Samples of the core, after the flooding, were inspected by Scanning Electron Microscopy (SEM) (Scanning Electron Microscope, VEGA, *TESCAN*). The core samples that were damaged in the process mentioned previously would develop a layer on their surface. A thin section of the damaged core was then cut at a thickness of one centimeter. These samples were then dried and viewed under the electron microscope. The SEM image enabled a three-dimensional view of the core sample at a microscopic level.

During this experiment, permeability was calculated from the measured pressure drop along the core through Darcy's law. According to Darcy's equation (*Eq. 1*), the permeability is dependent on the interfacial surface area, the viscosity, etc.:

$$Q = \frac{kA\Delta p}{\mu L} \quad (1)$$

2 MATHEMATICAL MODELING OF ASPHALTENE DEPOSITION IN POROUS MEDIA

The asphaltene deposition modeling is not only according to the mechanical plugging mechanism but also according to the asphaltene adsorption mechanism. In the majority of previous models, the asphaltene

TABLE 8
Experimental conditions for natural depletion tests

Test No.	Core sample	SWi (%)	SOi (%)	Q (cc/h)	Injection pressure (MPa)
1	3	36.7	63.3	1	–
2	3	36.7	63.3	3	–
3	3	36.7	63.3	10	–
4	3	36.7	63.3	30	–
5	3	36.7	63.3	40	–
6	4	37	63	10	–
7	1	43.7	56.3	1	–
8	1	43.7	56.3	5	–
9	2	43.7	56.3	3	–
10	1	43.7	56.3	–	41
11	1	43.7	56.3	–	44
12	1	43.7	56.3	–	48
13	1	43.7	56.3	–	50

TABLE 9
Considerations and parameters of the studied models

No.	Model	Ref.	Numbers of phases	Mechanisms of asphaltene deposition	Parameters
1	Proposed model (2012)	[28]	4	Multilayer adsorption equilibrium, surface deposition, entrainment of deposits and mechanical plugging	The first adsorption step parameter (this step is taken to be adsorption of asphaltenes in solution to the surface of the rock, the second adsorption step parameter (this step is taken to be the adsorption of asphaltenes in solution to those asphaltenes already adsorbed to the rock, the mean aggregation number of the adsorbed asphaltenes (in developed model), the maximum possible adsorption for the whole isotherm, surface deposition, entrainment of deposits, mechanical plugging, snowball-effect deposition constant and critical interstitial velocity of liquid phase parameters
2	Almehaideb (2004)	[8]	4	Monolayer adsorption equilibrium, surface deposition, entrainment of deposits and pore throat plugging	The adsorption parameter, the maximum possible adsorption for the whole isotherm, surface deposition, entrainment of deposits, mechanical plugging, snowball-effect deposition constant and critical interstitial velocity of liquid phase parameters
3	Wang and Civan (2001)	[7]	2	Surface deposition, entrainment of deposits and pore throat plugging	The surface deposition, entrainment of deposits and mechanical plugging, snowball-effect deposition constant and critical interstitial velocity of liquid phase parameters

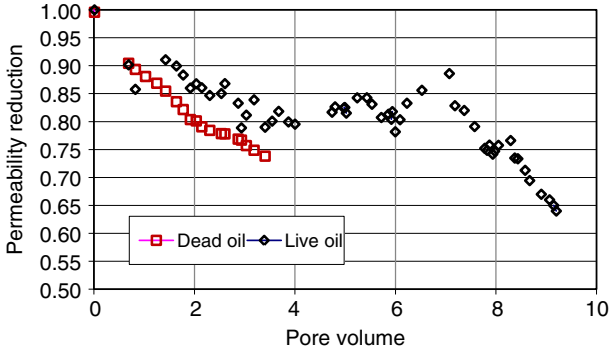

Figure 6

Permeability reduction for studied live reservoir fluid and dead residual oil *versus* the injected pore volume for a sandstone core sample.

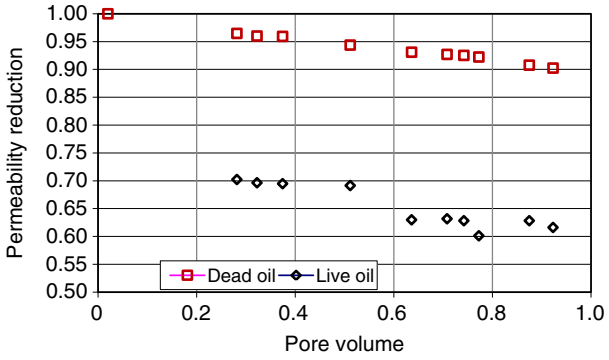

Figure 7

Permeability reduction for studied live reservoir fluid and dead residual oil *versus* the injected pore volume for a carbonate core sample.

deposition is based only on the mechanical trapping mechanism and it is different from the asphaltene adsorption mechanism. Also, the majority of previous work used two material balance equations based on the oil and asphaltene phases for core samples. In order to develop asphaltene deposition modeling including the asphaltene adsorption mechanism, a new model based on multilayer adsorption equilibrium theory and four material balance equations (oil, asphaltene, gas and water phases) was developed to account for asphaltene multilayer adsorption on core samples, as presented in our previous publication [28]. In this work, the results of asphaltene deposition in core samples during natural depletion were predicted using our proposed

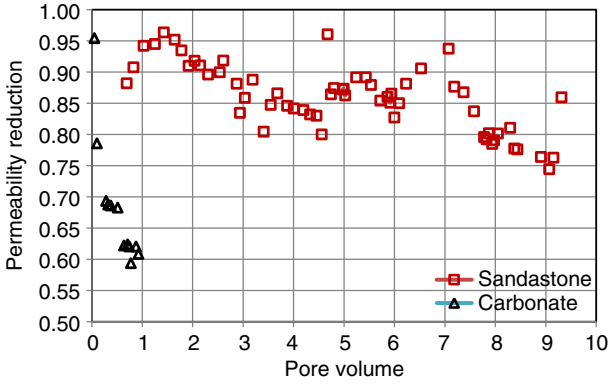

Figure 8

Permeability reduction *versus* the injected pore volume for studied live reservoir fluid.

model based on the multilayer adsorption equilibrium mechanism and compared with those obtained using asphaltene deposition modeling based on the monolayer adsorption equilibrium mechanism [8], and obtained by Wang and Civan's [7] model based only on the mechanical plugging mechanism.

2.1 Asphaltene Precipitation Model

Solid modeling treats the precipitating asphaltene as a single component residing in the solid phase, while the oil and gas phases are modeled with a cubic EOS. Solid models may require many empirical parameters and excessive tuning to match experimental data. In this study, the Nghiem model [29] was used; the fugacity of asphaltene in the solid phase is given by:

$$Inf_a = Inf_a^* + \frac{v_a(P - P^*)}{RT} \quad (2)$$

In a mixture, when the vapor, liquid and asphaltene phases coexist, the following thermodynamic equilibrium equations should be satisfied [29]:

$$lnf_{iv} = lnf_{il} \quad (3)$$

A three-phase flash algorithm is used to solve the above equations by using SRK EOS for the liquid and vapor phases. The existence of a solid phase satisfies the following criterion [29]:

$$f_{as} \geq f_{al} \quad (4)$$

In this model, the only parameter that should be adjusted from the experimental data is the referenced pressure, P^*. Also, according to our previous publication [30],

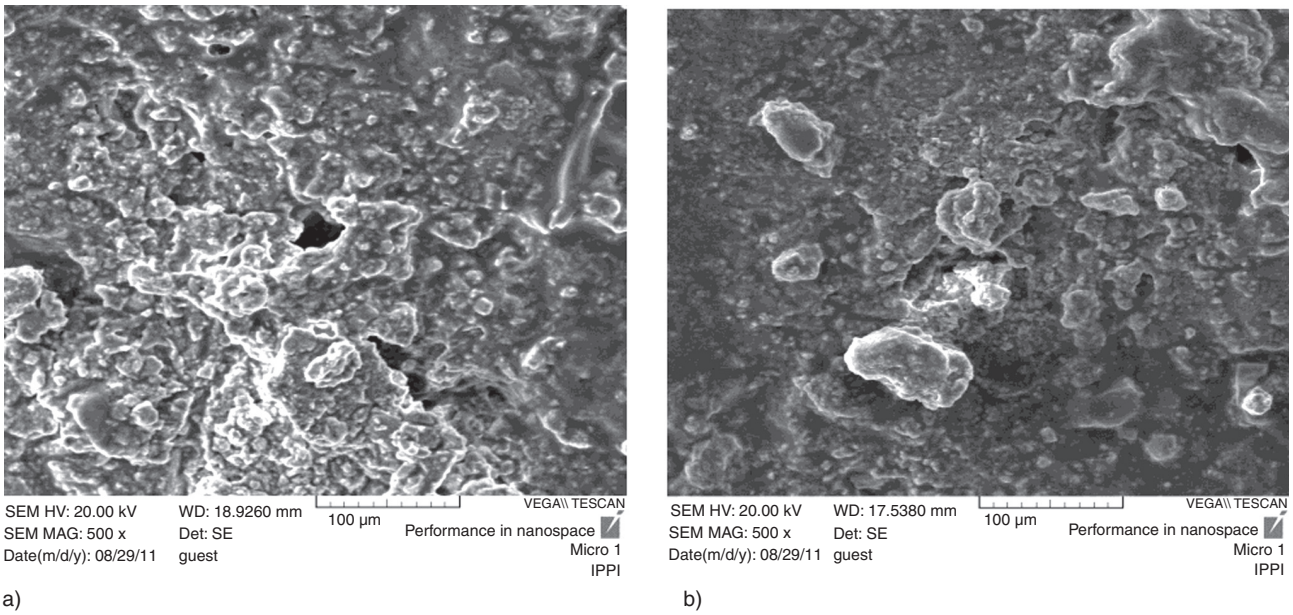

Figure 9

SEM images in studied a) carbonate and b) dolomite core samples.

the asphaltene precipitation in this bottom hole live oil was calculated based on the Flory-Huggins theory.

2.2 Asphaltene Adsorption and Deposition Models

There are two asphaltene deposition mechanisms on porous media, adsorption and mechanical plugging.

The asphaltene adsorption mechanism, which is related to the interactions between the asphaltene functional groups and the rock surface, involves surface polarity, affinity or other attractive forces. This process is reversible, with asphaltene desorbing from porous media when the concentration of suspended asphaltene in crude oil decreases. Asphaltene is a polar component; therefore, formations containing clay and carbonate formation have greater ability than sandstone formations to adsorb asphaltene.

In order to develop a new model for asphaltene deposition in porous media, a multilayer adsorption equilibrium term was included in the asphaltene flow rate and porosity relations, as presented in our previous publication [28]. In this model, two steps are considered for asphaltene adsorption. The first adsorption step is taken as the adsorption of asphaltenes in solution to the surface of the rock, and the second adsorption step is taken as the adsorption of asphaltenes in solution to those asphaltenes already adsorbed to the rock, as follows [31]:

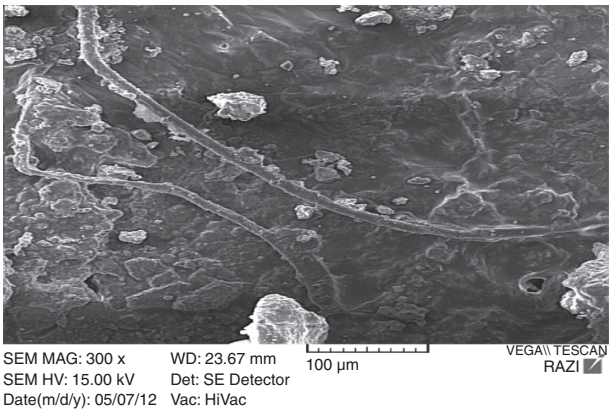

Figure 10

SEM image in studied sandstone core sample.

$$\Gamma = \frac{\Gamma_\infty k_1 C(n^{-1} + k_2 C^{n-1})}{1 + k_1 C(1 + k_2 C^{n-1})} \tag{5}$$

Also, by comparison, the asphaltene adsorption was modeled using a monolayer adsorption equilibrium term (Langmuir isotherm equation), as follows [8]:

$$W_{sa} = \frac{W_{sa,max}.K_a.C_{sf}}{K_a.C_{sf} + 1} \tag{6}$$

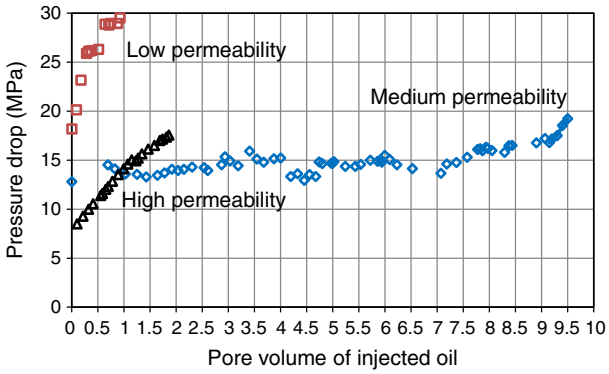

Figure 11

Variation of pressure drop *versus* injected pore volume for studied cores.

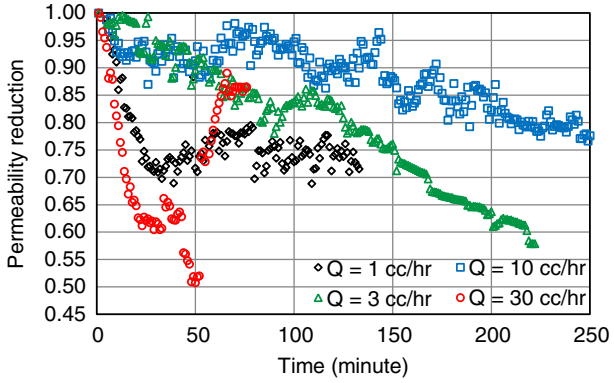

Figure 12

Effect of flow rate on permeability reduction in sandstone core sample (live reservoir fluid).

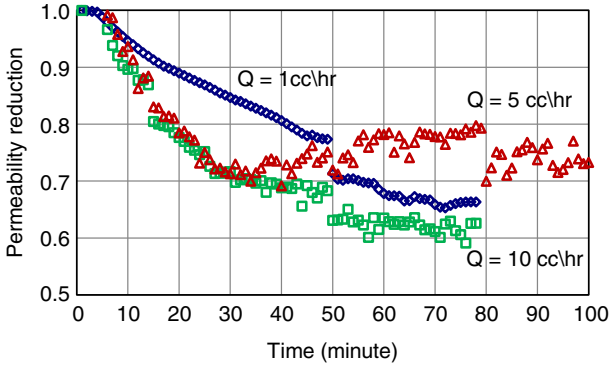

Figure 13

Effect of flow rate on permeability reduction in carbonate core sample (live oil).

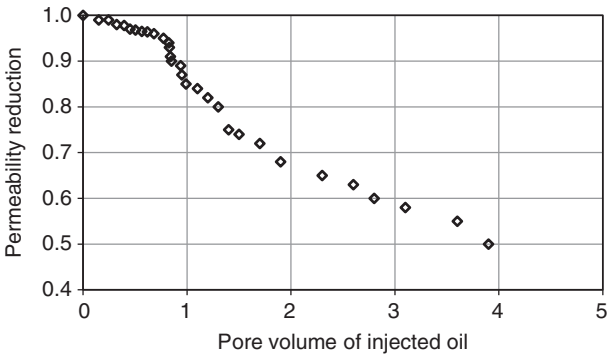

Figure 14

Effect of flow rate on permeability reduction in carbonate core sample (live oil).

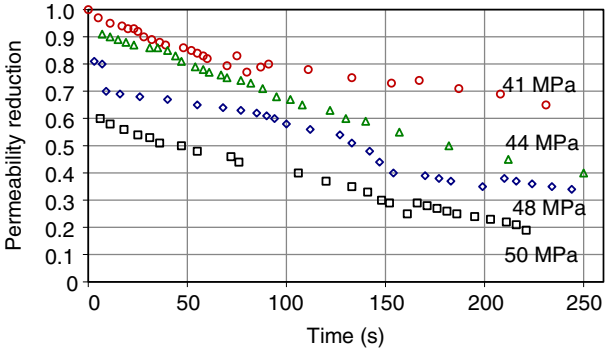

Figure 15

Effect of injection pressure on formation damage.

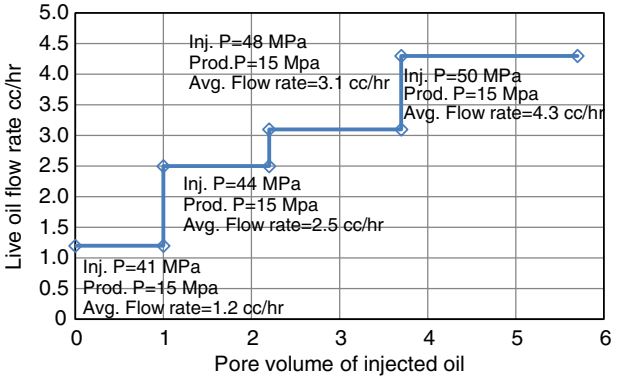

Figure 16

Variation of flow rates of live reservoir fluid recorded *versus* pore volume injected during flooding.

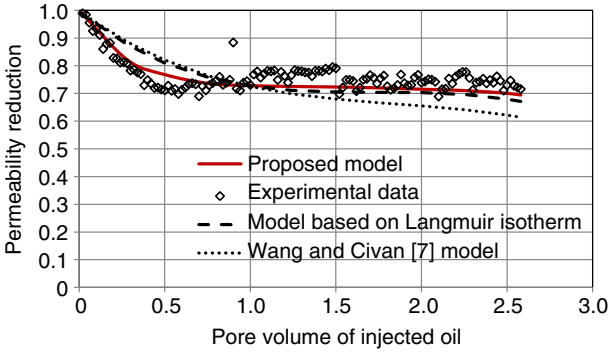

Figure 17

Experimental and simulated permeability reduction during primary deposition (Q = 1 cc/h) in sandstone core sample (live reservoir fluid).

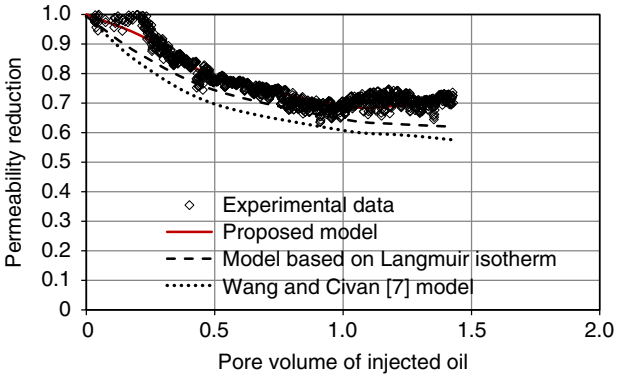

Figure 18

Experimental and simulated permeability reduction during primary deposition (Q = 1 cc/h) in carbonate core sample (live reservoir fluid).

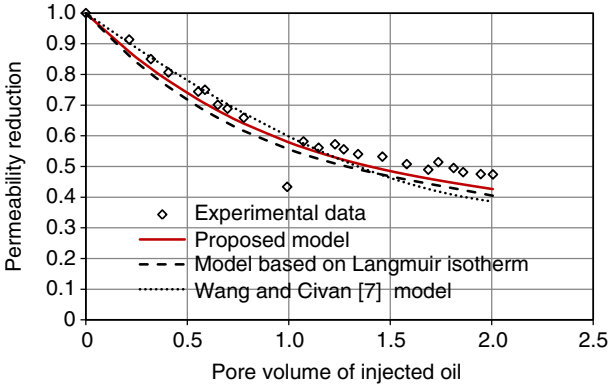

Figure 19

Experimental and simulated permeability reduction during primary deposition (Q = 3 cc/h) in dolomite core sample (live reservoir fluid).

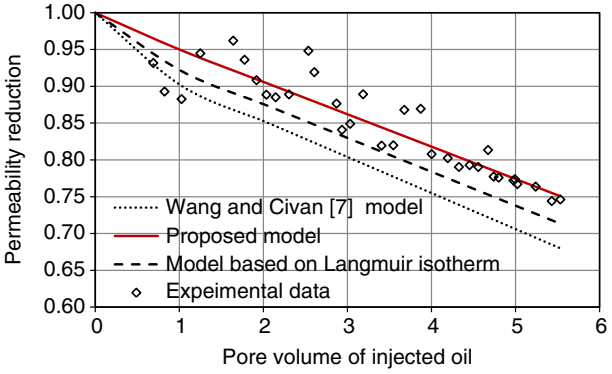

Figure 20

Experimental and simulated permeability reduction during primary deposition (Q = 10 cc/h) in sandstone core sample (live reservoir fluid).

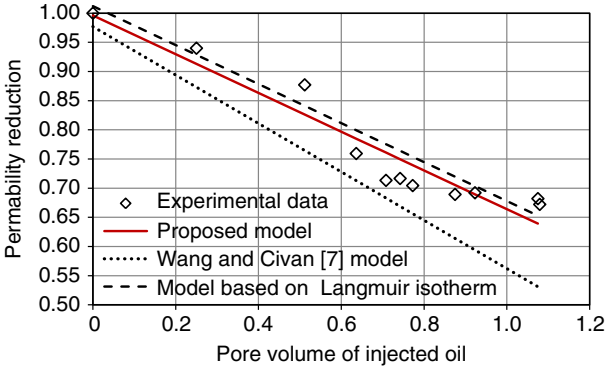

Figure 21

Experimental and simulated permeability reduction during primary deposition (Q = 10 cc/h) in carbonate core sample (live reservoir fluid).

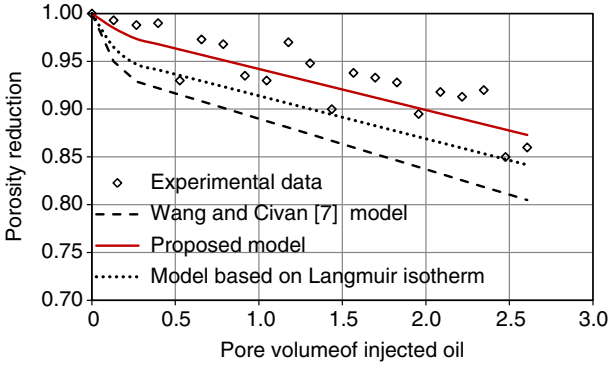

Figure 22

Experimental and simulated porosity reduction during primary deposition (Q = 1 cc/h) in sandstone core sample (live reservoir fluid).

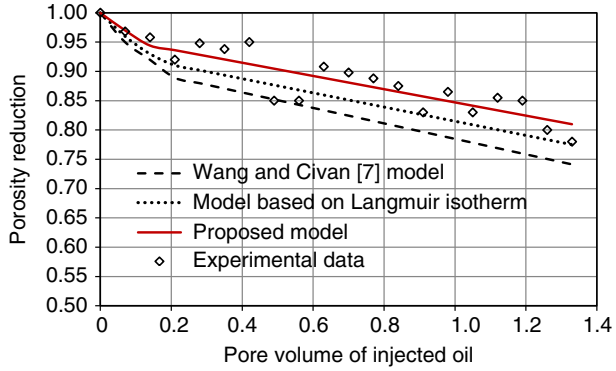

Figure 23

Experimental and simulated porosity reduction during primary deposition (Q = 1 cc/h) in carbonate core sample (live reservoir fluid).

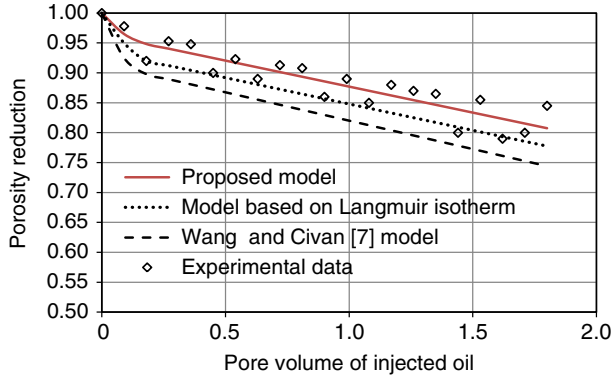

Figure 24

Experimental and simulated porosity reduction during primary deposition (Q = 3 cc/h) in dolomite core sample (live reservoir fluid).

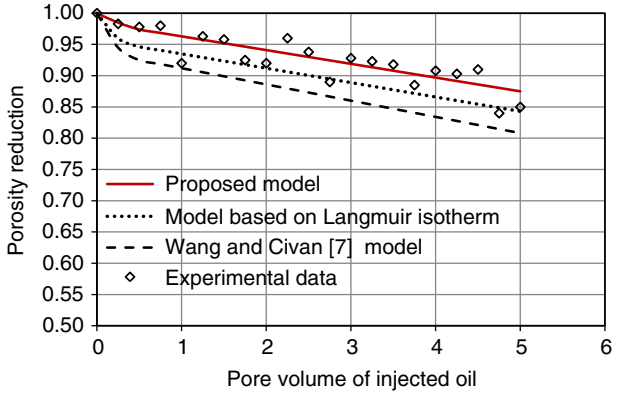

Figure 25

Experimental and simulated porosity reduction during primary deposition (Q = 10 cc/h) in sandstone core sample (live reservoir fluid).

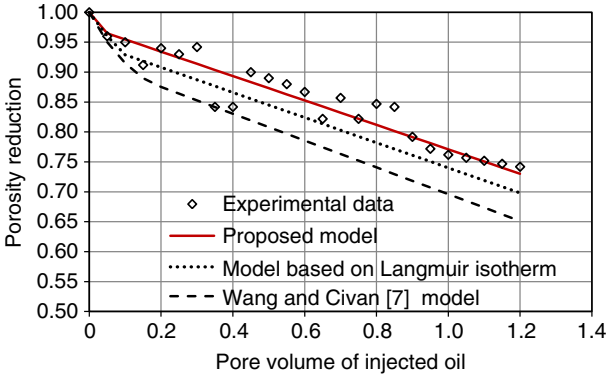

Figure 26

Experimental and simulated porosity reduction during primary deposition (Q = 10 cc/h) in carbonate core sample (live reservoir fluid).

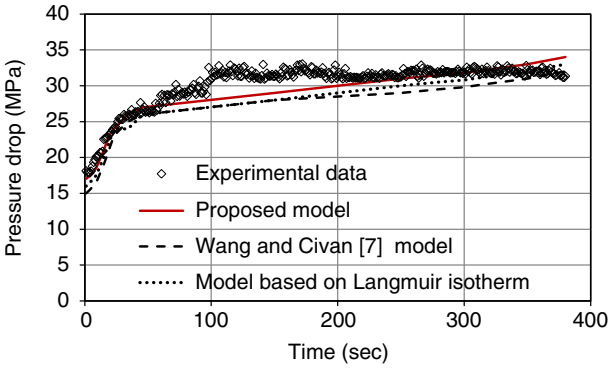

Figure 27

Experimental and simulated pressure drop during primary deposition (Q = 10 cc/h) in carbonate core sample (live reservoir fluid).

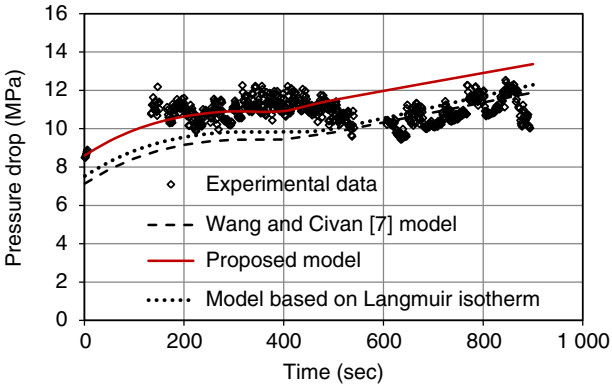

Figure 28

Experimental and simulated pressure drop during primary deposition (Q = 1 cc/h) in sandstone core sample (live reservoir fluid).

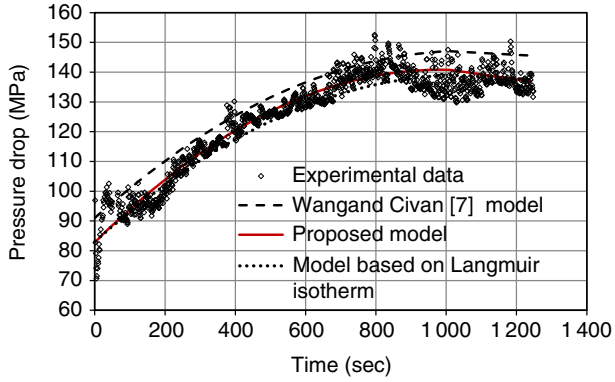

Figure 29

Experimental and simulated pressure drop during primary deposition (Q = 1 cc/h) in carbonate core sample (live reservoir fluid).

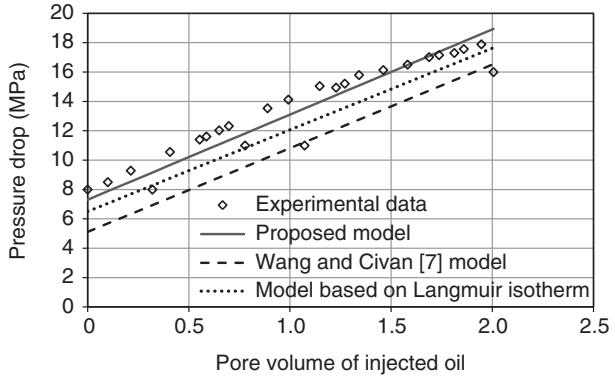

Figure 30

Experimental and simulated pressure drop during primary deposition (Q = 3 cc/h) in dolomite core sample (live reservoir fluid).

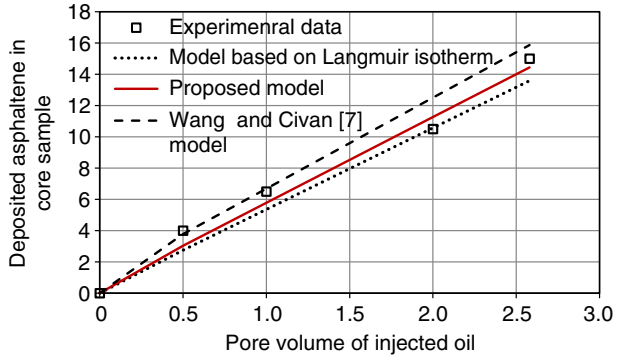

Figure 31

Experimental and simulated deposited asphaltene during primary deposition (Q = 3 cc/h) in dolomite core sample (live reservoir fluid).

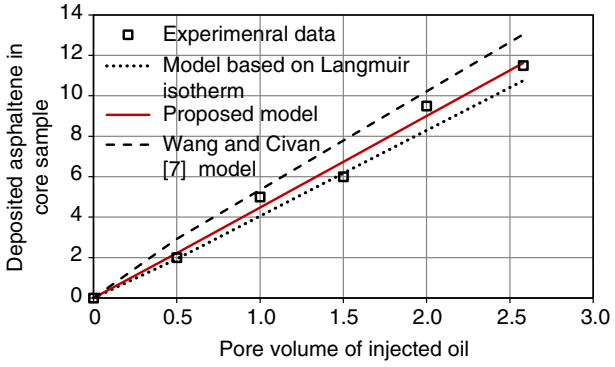

Figure 32

Experimental and simulated deposited asphaltene during primary deposition (Q = 1 cc/h) in sandstone core sample (live reservoir fluid).

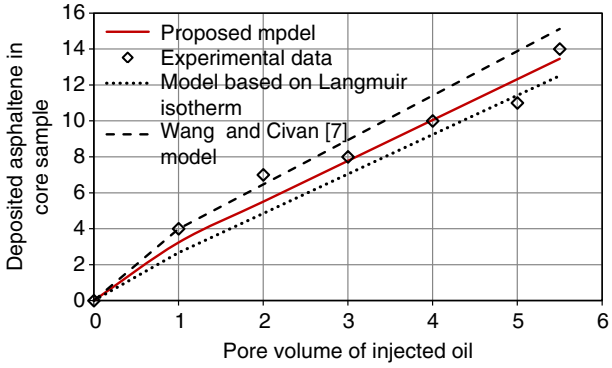

Figure 33

Experimental and simulated deposited asphaltene during primary deposition (Q = 10 cc/h) in sandstone core sample (live reservoir fluid).

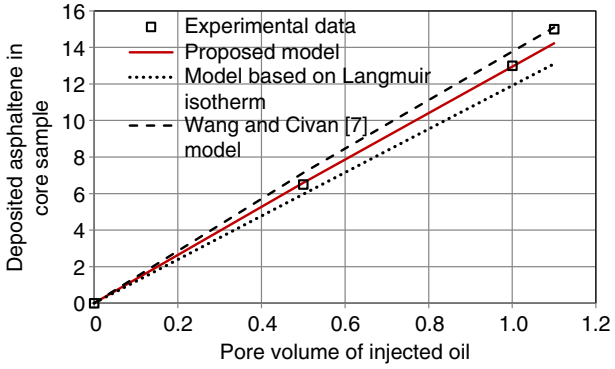

Figure 34

Experimental and simulated deposited asphaltene during primary deposition (Q = 10 cc/h) in carbonate core sample (live reservoir fluid).

The deposition rate for asphaltene is given by:

$$\frac{\partial E_A}{\partial t} = \alpha C_A \emptyset - \beta E_A (v_L - v_{cr,L}) + \gamma u_L C_A \qquad (7)$$

where the first term represents the surface deposition, the second term represents the entrainment of asphaltene deposits by the flowing phase when the interstitial velocity is larger than a critical interstitial velocity, and the last term represents the pore throat plugging rate. The value of β is set as [7]:

$$\begin{aligned} \beta &= \beta_i, \text{ when } v_L > v_{cr,L} \\ \beta &= 0, \text{ otherwise} \end{aligned} \qquad (8)$$

where v_L is equal to u_L/ϕ The value of γ is described as [7]:

$$\begin{aligned} \gamma &= \gamma_i(1 + \sigma E_A), \text{ when } D_{pt} < D_{ptcr} \\ \gamma &= 0, \text{otherwise} \end{aligned} \qquad (9)$$

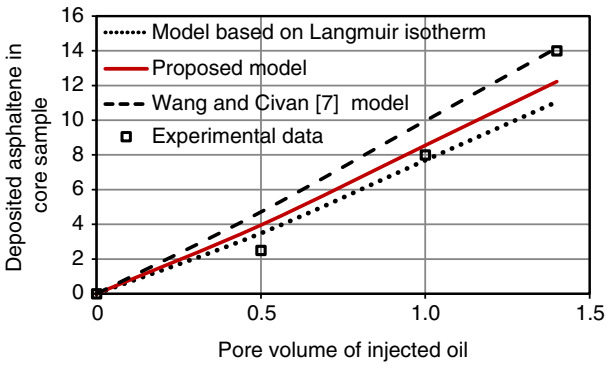

Figure 35

Experimental and simulated deposited asphaltene during primary deposition (Q = 1 cc/h) in carbonate core sample (live reservoir fluid).

Thus, the pore throat plugging deposition rate increases proportionally with the total deposits. When D_{pt} is less than D_{ptcr}, pore throat plugging deposition will occur. The details of these models are described else where [7].

2.3 Mass Balance Equations

The asphaltene precipitation and deposition problems are represented by mass balance equations for the liquid and asphaltene, the momentum balance equation, the asphaltene precipitation and deposition models, and the porosity and permeability reduction models [7].

The mass balance for asphaltene is given by [7]:

$$\frac{\partial}{\partial t}(\emptyset \rho_A C_A + \emptyset \rho_L W_{AL}) + \frac{\partial}{\partial x}(\rho_L u_L w_{SAL} + \rho_L u_L w_{AL}) = -\rho_A \frac{\partial}{\partial t} E_A \qquad (10)$$

The mass balance equation for the live oil phase is given by [7]:

$$\frac{\partial}{\partial t}(\emptyset \rho_L w_{OL}) + \frac{\partial}{\partial x}(\rho_L u_L w_{OL}) = 0 \qquad (11)$$

where O represents the oil component and L represents the liquid phase. The details of these models are described elsewhere [7].

The majority of previous work used two material balance equations based on the oil and asphaltene phases for core samples. The material balance equations are included for the water and gas components during flooding processes, and therefore the material balance equations are proposed as follows:

Gas phase [28]:

$$\frac{\partial}{\partial t}(\emptyset S_V \rho_G + \emptyset S_L \rho_L W_G) + \frac{\partial}{\partial x}(\rho_L u_L w_G + \rho_L u_G) = 0 \qquad (12)$$

TABLE 10

Absolute Average Deviation of the correlated permeability reduction from the experimental results by the proposed model and other models

	Absolute Average Deviation of asphaltene deposition modeling (%)								
Oil injection flow rate (cc/h)	Proposed model	Model based on monolayer adsorption equilibrium mechanism	Wang and Civan [7] model	Proposed model	Model based on monolayer adsorption equilibrium mechanism	Wang and Civan [7] model	Proposed model	Model based on monolayer adsorption equilibrium mechanism	Wang and Civan [7] model
	Sandstone core sample (3)			Carbonate core sample			Dolomite core sample		
1	2.8	3.5	4.2	3.1	3.5	5.6			
3	–	–	—	—		—	2.4	3.2	5.1
10	2.9	3.8	4.5	2.6	3.1	4.8	—		–

TABLE 11
Asphaltene deposition adjusted parameters of the proposed model in core samples

Adjusted parameter	Oil injection rate (cc/h)				
	Sandstone core sample		Carbonate core sample		Dolomite core sample
	1	10	1	10	3
α (1/s)	0.02	0.05	0.07	0.09	0.06
β (1/cm)	0.05	0.06	0.42	0.58	0.08
v_c (cm/s)	0.04	0.02	0.03	0.02	0.02
Γ (1/cm)	0.03	0.05	0.24	0.36	0.07
Γ_∞ (mg/g)	159.5	159.5	159.5	159.5	159.5
k_1	1.1×10^{-4}	1.1×10^{-4}	6.1×10^{-3}	9.1×10^{-3}	4.6×10^{-3}
k_2	4.6×10^{-9}	5.9×10^{-9}	8.9×10^{-8}	9.6×10^{-8}	4.3×10^{-8}
n	17	18	11	14	10
f_p	1	1	1	1	1
σ	32	36	41	45	38

Water phase [28]:

$$\frac{\partial}{\partial t}(\text{Ø}S_W\rho_W w_{WL}) + \frac{\partial}{\partial x}(\rho_W u_W w_{WL}) = 0 \tag{13}$$

The momentum balance equation is given by Darcy's law [7]:

$$u_L = -\frac{k}{\mu_L}\frac{\partial P}{\partial x} \tag{14}$$

The instantaneous local porosity during asphaltene deposition is equal to the difference between the initial porosity and the fractional pore volume occupied by the deposited asphaltene and adsorbed asphaltene [28]:

$$\text{Ø} = \text{Ø}_0 - E_A - E_{ad} \tag{15}$$

The instantaneous, local permeability, k, is calculated by [7]:

$$k = f_p k_0 \left(\frac{\text{Ø}}{\text{Ø}_0}\right)^m \tag{16}$$

Table 9 summarizes the considerations and parameters for all the studied models.

Experimental permeability damage due to asphaltene deposition in cores was correlated using the above model of asphaltene deposition and their coefficients were adjusted to achieve the best match with the experimental data. The partial differential equations were coupled and solved using a finite-difference method, backward both in time and space, in MATLAB software to determine pressure and asphaltene concentration in the core samples. The Runge-Kutta fourth-order scheme was applied to calculate the volume fraction of asphaltene deposition and adsorption. A fully implicit numerical model was performed and solved by iterations. Numerical simulation runs were conducted to obtain the best match between experimental and numerical results. Numerical simulation was carried out in a linear grid system of 90 grid blocks. Time was discretized with a Δt of 30 second. For optimization and determination of the model parameters, history matching was used. In this study, square roots of the summation of the differences between measured and calculated porosity data are defined as the objective function [28]:

$$\text{Objective Function} = \sqrt{\sum_{i=1}^{n}\left(\left(\frac{k}{k_0}\right)_{measured} - \left(\frac{k}{k_0}\right)_{calculated}\right)^2} \tag{17}$$

As a result, the model parameters obtained by the optimization procedure are Γ_∞, k_1, k_2, m, n, α, β, v_c, γ, K_a, σ and f_p.

The simulated data are not appreciably sensitive to time and space steps.

TABLE 12
Asphaltene deposition adjusted parameters of the model based on the Langmuir isotherm in core samples

Adjusted parameter	Oil injection rate (cc/h)				
	Sandstone core sample		Carbonate core sample		Dolomite core sample
	1	10	1	10	3
α (1/s)	0.02	0.04	0.06	0.08	0.06
β (1/cm)	0.04	0.05	0.38	0.62	0.09
v_c (cm/s)	0.04	0.02	0.03	0.02	0.02
γ (1/cm)	0.02	0.04	0.31	0.56	0.07
$w_{sa,max}$ (mg/g)	0.2	0.2	0.2	0.2	0.2
K_a	2 500	2 500	2 500	2 500	2 500
f_p	1	1	1	1	1
σ	31	34	43	48	37

TABLE 13
Asphaltene deposition adjusted parameters of Wang and Civan's [7] model in core samples

Adjusted parameter	Oil injection rate (cc/h)				
	Sandstone core sample		Carbonate core sample		Dolomite core sample
	1	10	1	10	3
α (1/s)	0.01	0.01	0.02	0.01	0.02
β (1/cm)	0.06	0.07	0.32	0.48	0.09
v_c (cm/s)	0.04	0.02	0.03	0.02	0.02
γ (1/cm)	0.018	0.03	0.54	0.75	0.05
f_p	1	1	1	1	1
σ	32	38	43	48	41

3 RESULTS AND DISCUSSION

3.1 Effect of Crude Oil Type on Asphaltene Deposition

Figures 6 and 7 show the permeability reduction of two sandstone and carbonate core samples *versus* the pore volume of injected live reservoir fluid and dead residual oil samples.

As observed, higher permeability reduction is caused when injecting the live reservoir fluid samples in comparison with the results obtained by injecting the dead residual oil samples for the studied sandstone and carbonate cores. This observation can be justified by the fact that the $C_{12}{}^{+}$ fraction in live reservoir fluid samples is heavier than the dead residual oil and contains more asphaltene content. Also, this difference may be from the state of asphaltene in live crude oil that is quite different from that in dead residual oil. It is clear that live and dead residual oil asphaltene show clear compositional differences, including [26]:

- the dead residual oil asphaltene sample contains a lower amount of the nitrogen-containing species but is higher in rings plus double bonds in comparison with the live reservoir asphaltene sample;
- the live reservoir asphaltenes are rich in sulfur and oxygen compared with the dead residual oil asphaltene;
- the live reservoir asphaltene has less aromatic compounds compared with the dead residual oil asphaltene;
- the live oil asphaltene contains more functional groups and less saturated groups in comparison with the dead oil asphaltene.

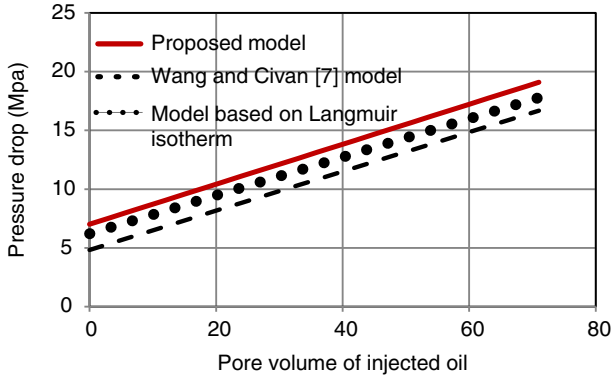

Figure 36

Pressure drop *versus* pore volume oil injected for oil GF3.

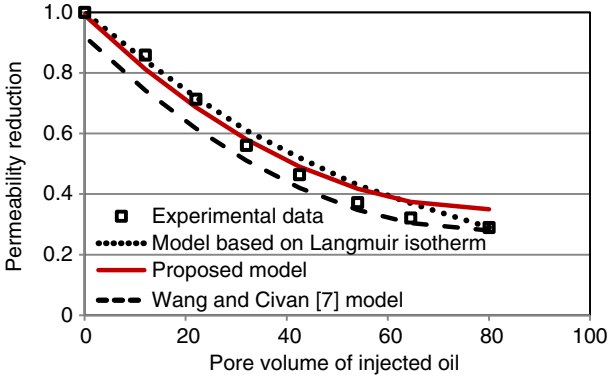

Figure 39

Permeability reduction *versus* pore volume oil injected for oil GF3.

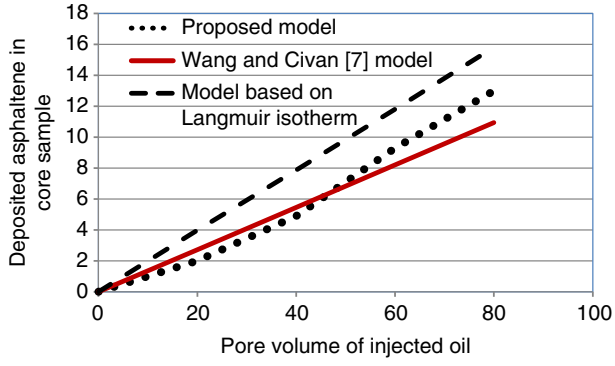

Figure 37

Deposited asphaltene in core sample *versus* pore volume of injected oil.

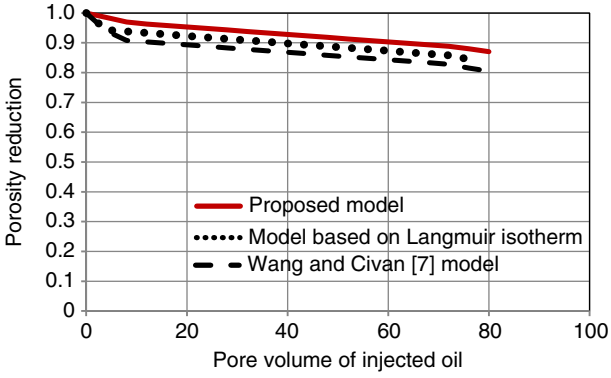

Figure 40

Porosity reduction *versus* pore volume oil injected for oil GF3.

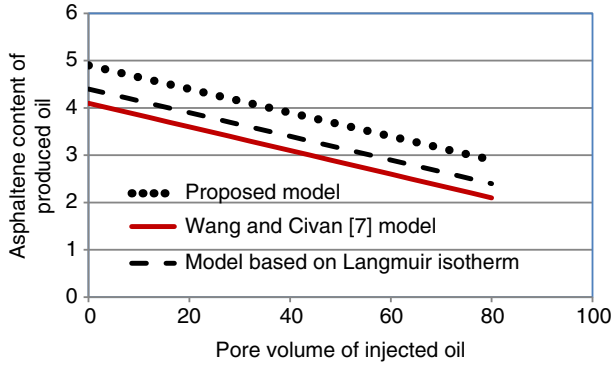

Figure 38

Asphaltene content of produced oil *versus* pore volume of injected oil.

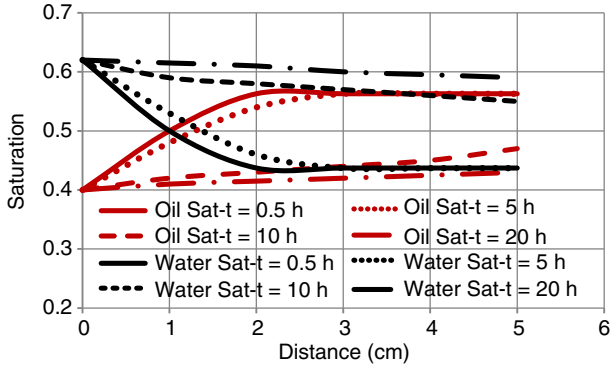

Figure 41

Saturation profiles at different time steps in carbonate core sample (Q = 1 cc/h).

Based on these results, it was concluded that the propensity for the asphaltenes of live reservoir fluid to aggregate into larger particles and to deposit on the rock was higher than for asphaltenes of dead residual oil. Therefore, permeability reduction and formation damage by asphaltene deposition during live reservoir fluid flooding were higher than for the dead residual oil flooding.

3.2 Effect of Rock Type on Asphaltene Deposition

Figure 8 shows the variation of the permeability for different types of core samples at various pore volumes of the injected live reservoir fluid.

As can be seen from this figure, the permeability reduction in carbonate rock types is steeper than that observed in sandstone rock cores over the whole range of pore volume numbers. Also, it can be observed that the carbonate core samples can be plugged at lower pore volume numbers due to the higher rate of asphaltene deposition and permeability reduction. Thus, it can be found that the plugging deposition mechanism is very significant in asphaltene deposition in carbonate core samples.

The SEM images for both carbonate and sandstone rock types are given in Figures 9 and 10. As shown in these figures, a comparison of SEM images revealed that the carbonate core samples would develop a layer on their surface. Thus, the carbonate core samples experienced more particle plugging compared with sandstone core samples, and the carbonate core samples were severely plugged by aspaltene deposition. It can be seen that asphaltene deposition has different mechanisms in carbonate and sandstone core samples. Therefore, it can be concluded that the adsorption mechanism in asphaltene deposition in carbonate core samples is more significant than that in sandstone core samples.

The difference between the carbonate and the sandstone cores is related to the core structure, mineral composition and consolidation. Hence, the carbonate core's inner surface may contain polar groups, which can exert polar interactions with asphaltene surface groups. Therefore, it is likely that asphaltene deposition on the carbonate core's surface can involve π-interaction and hydrogen bonding between the asphaltene groups and core surface polar groups. Asphaltene is a polar component: therefore, formations containing clay and carbonate have greater ability than sandstone formations to adsorb asphaltene [23]. In fact, the existence of polar components makes the asphaltene molecules adhere more strongly to the surface, and hence increases the amount of asphaltene deposition on the surface of the carbonate rock samples.

Figure 11 indicates the pressure drop *versus* pore volume for three rocks with different permeability.

It can be concluded that the formation damage caused by asphaltene deposition in low-permeability rock was more severe than that in higher-permeability rock for the same asphaltene content of the crude oil and under the same dynamic potential force. For low-permeability core samples, there may be a continuous deposition until complete plugging. In low-permeability cores, the plugging mechanism acts like a snowball growth that can be inferred from the sharp slopes of Figure 11 once plugging deposition is activated, leading to the first significant pressure variation. The results indicated that in low-permeability cores, the region of the asphaltene deposition was spread. There may also be a slow steady plugging for high-permeability cores. Furthermore, the deposition of asphaltene in the core was lower. In the high-permeability core, the region of the asphaltene deposition was limited in the inlet end of the core. Finally, a steady deposition can occur until interstitial velocity is high enough to not allow further mechanical plugging for medium permeability cores.

3.3 Effect of Oil Injection Flow Rate on Asphaltene Deposition

Figures 12-14 show the plot of the permeability reduction as a function of time for the cases of 1 to 30 cc/h injection rates for sandstone cores and 1 to 10 cc/h injection rates for carbonate cores.

One of the most important results from this experiment is the permeability reduction of the core samples at the beginning of the injection, which shows that the plugging of the pore throats occurs immediately after asphaltene deposition. The results also show that the asphaltene deposition on the covered pore surface with asphaltene layers is less than that on the clean surface.

These plots clearly show that an increase in flow rate is followed by an increase in asphaltene deposition at low flow rates. At these flow rates, the permeability reduction took place in a steady manner. The reduction continued until a steady state was reached. At this point, the relatively low deposition rate leads to the development of a steady state in pores. Also, these figures show that reduction in permeability until a minimum value was observed, and then a reversal in permeability reduction took place at higher flow rates. At this point, the permeability increased and reached a steady state. For this case, flow begins with a speed

higher than the critical speed but it declines steadily below the critical velocity and the asphaltene deposits. Because of asphaltene deposition, the pores are blocked and the speed increases beyond the critical speed and the entrainment phenomenon begins, resulting in an increasing permeability.

Figure 14 shows that at a higher flow rate, 40 cc/h, the asphaltene plugging process appeared to begin late.

However, as the flow continued, permeability reduction took place very quickly. For this case, a steady-state condition was never reached, and the injection pressure continued to rise until the injection had to be stopped. For this case, local speed values remain above the critical speed. Consequently, permeability reduction remains steady. This also means that most asphaltenes trapped would be in the vicinity of the wellbore, an area that can be treated with production stimulation operations [6].

3.4 Effect of Production Pressure on Permeability Reduction

Figure 15 shows the effect of production pressure on permeability reduction as a function of time.

It can be seen from this figure that the highest permeability reduction occurs at the highest production pressure at 50 MPa. The damage of the core sample was found to increase when the production pressures were increased. At higher production pressures, the asphaltene deposition in the core sample increased due to the increase in the driving force acting on the asphaltene particles. Greater asphaltene deposition caused severe blockage of pore throats, and thus greater reduction in permeability of the core sample induced.

Also, at high pressures, the asphaltenes are soluble in oil. However, during pressure depletion, the oil expands, reducing the oil solubility parameter, and it becomes a poor solvent for asphaltene. At a low pressure, asphaltenes begin to precipitate. Pressure depletion is the main reason for asphaltene deposition due to the destabilization of asphaltenes. This phenomenon occurred due to the decrease in the crude oil density, the vaporization of the light component and the decrease in the solubility of asphaltenes in the oil [32].

The flow rates of live reservoir fluid recorded for each injection pressure during the live reservoir fluid flooding experiment are shown in Figure 16.

It is seen that the recorded flow rates were in continuous response to the imposed pressure drops. In other words, a decrease in the system pressure was followed almost immediately or instantaneously, by a resulting increase in the system flow rate. This behavior indicates that an increase in injection pressure is followed by a constant production pressure.

3.5 Modeling Approach

In the majority of previous models, the asphaltene deposition is based on the mechanical plugging mechanism [7] and also, only two material balance equations were applied. Therefore, the previous models in the literature do not consider the adsorption mechanism, which is related to interactions between the positive polar component of asphaltenes and the rock surface.

Therefore, in the proposed asphaltene deposition model [28], in addition to the mechanical plugging mechanism term, a multilayer adsorption equilibrium mechanism term for asphaltene was included. Also, application of four material balance equations (oil, asphaltene, gas and water phases) instead of two material balance equations was considered. In this section, the results of asphaltene deposition in core samples during natural depletion were predicted using our proposed model based on the multilayer adsorption equilibrium mechanism and compared with those obtained using asphaltene deposition modeling based on the monolayer adsorption equilibrium mechanism [8] and obtained by Wang and Civan's [7] model based only on the mechanical plugging mechanism.

The proposed model was correlated using the natural depletion experimental data obtained in this work which are denoted as 1 to 12 in Table 8.

Figures 17 to 35 show the results of permeability reduction, porosity reduction, pressure drop and deposited asphaltene in the sandstone, carbonate and dolomite core samples due to asphaltene deposition using the proposed model and compared with those obtained using asphaltene deposition modeling based on the monolayer adsorption equilibrium mechanism [8] and obtained by Wang and Civan's [7] model based only on the mechanical plugging mechanism.

Figures 17 to 35 show that the proposed model can correlate the experimental data more accurately in comparison with the Wang and Civan [7] model and the model based on the monolayer adsorption equilibrium mechanism. These figures show that reduction in permeability until a minimum value was observed and then permeability increased in the experimental data. Because of asphaltene deposition, the pores are blocked and the speed increase beyond the critical speed and the entrainment phenomenon begins, resulting in increasing permeability.

Figures 22 to 26 compare the results of porosity reduction due to asphaltene deposition in core samples using the proposed model with those obtained from the Wang

and Civan [7] model and the model based on the monolayer adsorption equilibrium mechanism. It should be noted that the reduction of the porosity ratio is much lower than that of the permeability ratio.

Figures 27 to 30 compare the results of pressure drop in core samples during oil flooding due to asphaltene deposition using the proposed model with those obtained from the Wang and Civan [7] model and the model based on the monolayer adsorption equilibrium mechanism.

Figures 31 to 35 compare the results of deposited asphaltene in core samples during oil flooding using the proposed model with those obtained from the Wang and Civan [7] model and the model based on the monolayer adsorption equilibrium mechanism.

Table 10 shows the Average Absolute Deviation (AAD) of the predicted permeability reduction from the experimental data due to asphaltene deposition using the proposed model, that of the Wang and Civan [7] model, and that of the model based on the monolayer adsorption equilibrium mechanism. These results also confirm that the proposed model based on the multilayer adsorption equilibrium mechanism of asphaltene can correlate the permeability reduction experimental data with AAD of 2.4-3.1%, whereas the Wang and Civan [7] model correlates asphaltene deposition less accurately with AAD of 4.2-5.6%. This suggests that the multilayer adsorption mechanism of asphaltene has an important role in asphaltene deposition on core samples.

The results show that modeling based on the monolayer adsorption equilibrium mechanism is less accurate in the modeling of asphaltene deposition during natural depletion with AAD of 3.1-3.8%. Therefore, the asphaltene adsorption behavior on core samples is far from the monolayer adsorption equilibrium mechanism and is closer to the modified model based on multilayer adsorption equilibrium behavior.

This phenomenon can be explained by the fact that the asphaltene adsorption mechanism, which is related to the interactions between the asphaltene functional groups and the core surface, involves surface polarity, affinity or other attractive forces. It is also known that asphaltene surface groups may have acidic (carboxylic, benzoic, phenolic), and/or basic (pyridine, pyrazine, dimethylsulfoxide) functionality [23].

Tables 11 to 13 show the adjusted parameter values of the proposed model based on the multilayer adsorption equilibrium mechanism of asphaltene, the model based on the Langmuir isotherm and Wang and Civan's [7] model during natural depletion in core samples. It should be noted that the adjusted parameters are affected by the nature of core samples (rock morphology, rock-surface characteristics, mineral composition, etc.). For example, the adjusted parameters in the proposed model such as the first adsorption step parameter (k_1) and the second adsorption step parameter (k_2) have different quantities in carbonate and sandstone core samples, which is related to different mineral composition and rock morphology. Also, the results show that the second adsorption step parameter (k_2) is much lower than the first adsorption step parameter (k_1). It was found that the tendency for asphaltene deposition on the pore surface that was covered with asphaltene is less than that for the clean surface of core samples.

3.6 Case Study

In order to verify the accuracy of the proposed asphaltene deposition model, the model was run using the data given by Minssieux *et al.* [10], as denoted GF3. Figures 36 to 40 compare the results of the pressure drop, deposited asphaltene in the porous rock, remaining asphaltene concentration in the flowing oil, and permeability and porosity profiles at various times using the proposed model with those obtained from the Wang and Civan [7] model and the model based on the monolayer adsorption equilibrium mechanism. It should be noted that the deposition model constants given in Tables 11 to 13 are used in the above-mentioned models without using the GF3 experimental data.

The water and live oil saturation profiles were studied and the results are shown in Figure 41. The water saturation increases through the core sample. The water saturation increases from an initial value of 0.44 toward the value of 0.62. The oil saturation decreases through the core sample. The oil saturation reduces from an initial value of 0.56 toward the value of 0.4.

CONCLUSION

In this work, a set of experiments was conducted using bottom hole live oil samples under dynamic conditions in porous media with the purpose of investigation of asphaltene deposition and adsorption mechanisms involved in the interfacial interaction of the asphaltene/mineral rock. The effective parameters of porous media on asphaltene deposition, such as morphology of the surface, were studied in this work using SEM micrographs. Also, the experimental data obtained in this work were correlated by an asphaltene deposition model based on the multilayer adsorption equilibrium mechanism and four material balance equations (oil, asphaltene, gas and water phases) and the correlation results were compared with other models based on the mechanical plugging mechanism and the

monolayer adsorption equilibrium mechanism to account for permeability reduction in porous media in dynamic conditions. While none of the studied models cover the experimental results with satisfaction, the proposed model correlates the experimental formation damage data due to asphaltene deposition better in comparison with the other studied models.

The experimental and modeling results of asphaltene deposition and adsorption during core flooding led to the following conclusions:

- the proposed model, based on the multilayer adsorption equilibrium mechanism of asphaltene and four material balance equations, is found to be more accurate than Wang and Civan's [7] model based on the mechanical plugging mechanism with AAD of less than 3.2. Hence, the multilayer adsorption equilibrium mechanism of asphaltene has an important role in asphaltene deposition, permeability reduction and wettability alteration of reservoir rock;
- the experimental results showed that an increase in flow rate is followed by an increase in asphaltene deposition; permeability reduction and porosity reduction took place in a monotonous manner until a steady-state condition was reached at low flow rates. At higher flow rates, initial permeability was reduced until a minimum value and then an increase in permeability was observed until a steady-state condition was reached;
- the effect of rock type on asphaltene deposition was also studied. It can be seen that the asphaltene deposition has different mechanisms in carbonate and sandstone core samples. SEM micrographs of asphaltene deposition on the surface of carbonate core samples show the formation of large clusters and propose multilayer adsorption of asphaltene;
- the experimental results showed that the permeability reduction rate using the live reservoir fluid samples obtained from wells can be different from that of the same dead oil samples in the same conditions due to higher asphaltene content;
- as inferred, the experimental results indicated that three depositional types, continuous deposition for low-permeability cores, slow, steady plugging for high-permeability cores and steady deposition for medium-permeability cores, can be observed. The results showed that the values of pore volumes of the injected crude oil are higher for sandstone cores compared with carbonate cores;
- also, the experimental results showed that the damage of the core sample was found to increase when the injection pressure was increased;
- the proposed model was verified using experimental data reported in the literature.

ACKNOWLEDGMENTS

This research is sponsored by the Research Institute of Petroleum Industry (RIPI). This is gratefully acknowledged.

REFERENCES

1 Mullins O.C., Sheu E.Y., Hammami A., Marshal A.G. (2007) Asphaltene Self-Association and Precipitation in Solvents-AC Conductivity Measurements, in *Asphaltenes, Heavy Oils and Petroleomics*, Springer, New York.

2 Civan F., Knapp R.M., Ohen H.A. (1989) Alteration of Permeability by Fine Particles Processes, *J. Petrol. Sci. Eng.* **3**, 65-79.

3 Rassamdana H., Dabir B., Nematy M., Farhani M., Sahimi M. (1996) Asphalt Flocculation and Deposition: I, *The Onset of Precipitation, AICHE J.* **42**, 1, 10-21.

4 Andersen S.I., Speight J.G. (1999) Thermodynamic models for asphaltene solubility and precipitation, *J. Petrol. Sci. Eng.* **22**, 53-66.

5 Hu Y.F., Li S., Liu N., Chu Y.P., Park S.J., Mansoori G. A., Guo T.M. (2004) Measurement and corresponding states modeling of asphaltene precipitation in Jilin reservoir oils, *J. Petrol. Sci. Eng.* **41**, 169-182.

6 Ali M.A., Islam M.R. (1997) The effect of asphaltene precipitation on carbonate rock permeability: An experimental and numerical approach, *SPE Annual Technical Conference and Exhibition*, San Antonio, 5-6 Oct.

7 Wang S., Civan F. (2001) Productivity decline of vertical and horizontal wells by asphaltene deposition in petroleum reservoirs, *SPE International Symposium on Oilfield Chemistry*, Houston, Texas, 13-16 Feb., *SPE paper* 64991.

8 Almehaideb R.A. (2004) Asphaltene precipitation and deposition in the near wellbore region: a modeling approach, *J. Petrol. Sci. Eng.* **42**, 157-170.

9 Minssieux L. (1997) Core Damage from Crude Asphaltene Deposition, *SPE International Symposium on Oilfield Chemistry*, Houston, Texas, 18-21 Feb., *SPE* 37250.

10 Minssieux L., Nabzar L., Chauveteau G., Longeron D., Bensalem R. (1998) Permeability damage due to asphaltene deposition experimental and modeling aspects, *Oil Gas Sci. Technol. – Rev. IFP* **53**, 3, 313-327.

11 Papadimitriou N.I., Romanos G.E., Charalambopoulou G.C., Kainourgiakis M.E., Katsaros F.K., Stubos A.K. (2007) Experimental investigation of asphaltene deposition mechanism during oil flow in core samples, *J. Petrol. Sci. Eng.* **57**, 281-293.

12 Mendoza de la Cruz J.L., Castellanos-Ramirez I.V., Ortiz-Tapia A., Buenrostro-Gonzalez E., Duran-Valencia C., de los A., Lopez-Ramirez S. (2009) Study of monolayer to multilayer adsorption of asphaltenes on reservoir rock minerals, *Colloids Surf. A: Physicochem. Eng. Aspects* **340**, 149-154.

13 Buckley J.S. (1998) Wetting Alternation of Solid Surfaces by Crude Oils and their Asphaltenes, *Oil Gas Sci. Technol. – Rev. IFP* **53**, 3, 303-312.

14 Leontaritis K.J. (1989) Asphaltene deposition: A comprehensive description of problem manifestations and modeling approaches, *SPE Production Operations Symposium*, Oklahoma, City, 13-14 March.

15 Srivastava R.K., Huang S.S., Mingzhe D. (1999) Asphaltene Deposition during CO_2 Flooding, *SPE Prod. Facil.* **14**, 4, 235-245.

16 Kocabas I., Islam M.R., Modarress H. (2000) A wellbore model for field-scale modeling of asphaltene plugging, *J. Petrol. Sci. Eng.* **26**, 19-30.

17 Mendoza de la Cruz J.L., Argüelles-Vivas F.J., Matias-Perez V., Duran-Valencia C., de los A., Lopez-Ramirez S. (2009) Asphaltene-Induced Precipitation and Deposition During Pressure Depletion on a Porous Medium: An Experimental Investigation and Modeling Approach, *Energy Fuels* **23**, 5611-5625.

18 Civan F. (1995) Modeling and Simulation of Formation Damage By Organic Deposition, *First International Symposium in Colloid Chemistry in Oil Production: Asphaltenes and Wax Deposition, JSCOP'95*, Rio de Janeiro, Ri, Brazil, 26-29 Nov.

19 Jafari Behbahani T., Ghotbi C., Taghikhani V., Shahrabadi A. (2011) Investigation of Asphaltene Deposition Mechanisms During Primary Depletion and CO_2 Injection, *European Formation Damage Conference*, The Netherlands, 7-10 June.

20 Gruesbeck C., Collins R.E. (1982) Entrainment and deposition of fine particles in porous Media, *Soc. Pet. Eng. J.* **22**, 847-856.

21 Monteagudo J.E.P., Rajagopal K., Lage P.L.C. (2002) Simulating oil flow in porous media under asphaltene deposition, *Chem. Eng. Sci.* **57**, 323-337.

22 Nasri Z., Dabir B. (2010) Modeling of carbonate oil reservoirs in imbibition displacement with considering asphaltene deposition, *J. Petrol. Sci. Eng.* **70**, 273-281.

23 Hamadou R., Khodja M., Kartout M., Jada A. (2008) Permeability reduction by asphaltenes and resins deposition in porous media, *Fuel* **87**, 2178-2185.

24 Leontaritis K., Mansoori G. (1988) Asphaltene Deposition: A Survey of Field Experiences and Research Approaches, *J. Petrol. Sci. Eng.* **1**, 229-239.

25 Bagheri M.B., Kharrat R., Ghotbi C. (2011) Experimental Investigation of the Asphaltene Deposition Process during Different Production Schemes, *Oil Gas Sci. Technol. – Rev. IFP* **66**, 3, 507-519.

26 Klein G.C., Kim S., Rodgers R.P., Marshall A.G. (2006) Mass Spectral Analysis of Asphaltenes. I. Compositional Differences between Pressure-Drop and Solvent-Drop Asphaltenes Determined by Electrospray Ionization Fourier Transform Ion Cyclotron Resonance Mass Spectrometry, *Energy Fuels* **20**, 1965-1972.

27 Carbognani L., Izquierdo A. (1989) Preparative and automated compound class separation of venezuelan vacuum residua by high performance liquid chromatography, *J. chromatography* **484**, 399-405.

28 Jafari Behbahani T., Ghotbi C., Taghikhani V., Shahrabadi A. (2012) Investigation on Asphaltene Deposition mechanisms during CO_2 Flooding processes in porous media: A novel Experimental study and a modified model based on multilayer theory for asphaltene adsorption, *Energy Fuels* **26**, 5080-5091.

29 Nghiem L., Coombe D.A. (1997) Modeling Asphaltene Precipitation during Primary Depletion, *SPE J.* **2**, 170-176.

30 Jafari Behbahani T., Ghotbi C., Taghikhani V., Shahrabadi A. (2011) Experimental investigation and thermodynamic modeling of asphaltene precipitation, *Scientia Iranica C.* **18**, 6, 1384-1390.

31 Zhu B.-Y., Gu T. (1990) Reverse hemimicelle formation of 1-decanol from heptane at the solution/graphite interface, *Colloids Surf.* **46**, 339-345.

32 Vargas F.M., Gonzalez D.L., Hirasaki G.J., Chapman W. G. (2009) Modeling Asphaltene Phase Behavior in Crude Oil Systems Using the Perturbed Chain Form of the Statistical Associating Fluid Theory (PC-SAFT) Equation of State, *Energy Fuels* **23**, 1140-1146.

Manuscript accepted in February 2013
Published online in September 2013

Cite this article as: T.J. Behbahani, C. Ghotbi, V. Taghikhani and A. Shahrabadi (2013). Experimental Study and Mathematical Modeling of Asphaltene Deposition Mechanism in Core Samples, *Oil Gas Sci. Technol* **70**, 6, 1051-1074.